"This is a post-peer-review, pre-copyedit version of an article published in Journal of The American Society for Mass Spectrometry. The final authenticated version is available online at: https://doi.org/10.1007/s13361-017-1679-y "

Structural characterization of neutral saccharides by negative ion MALDI mass spectrometry using a superbasic proton sponge as deprotonating matrix

C.D. Calvano*[1,2], T.R.I. Cataldi[1,2], J. F. Kögel[3,4], A. Monopoli[1], F. Palmisano[1,2], J. Sundermeyer[3]

[1]Dipartimento di Chimica and [2]Centro di Ricerca Interdipartimentale SMART -Università degli Studi di Bari Aldo Moro, via Orabona 4, 70126 Bari (Italy)

[3]Fachbereich Chemie, Philipps-Universität Marburg, Hans-Meerwein-Straße, 35032 Marburg (Germany)

[4]FB Biologie/Chemie, Universität Bremen, Leobener Str. im NW2, 28359 Bremen, Germany

Number of Tables: 1
Number of Schemes: 3
Number of Figures: 7
Supplemental Material: Yes

Keywords: neutral saccharides, cyclodextrins, alditols, MALDI-mass spectrometry, superbasic proton sponge, tandem MS.

* Author for correspondence, cosimadamiana.calvano@uniba.it

Abstract

The superbasic proton sponge 1,8-bis(tripyrrolidinylphosphazenyl)naphthalene (TPPN) has been successfully employed for the structural characterization of neutral saccharides, cyclodextrins and saccharide alditols by matrix assisted laser desorption/ionization tandem mass spectrometry (MALDI-MS/MS). Due to its inherently high basicity, TPPN is capable of deprotonating neutral carbohydrates (M) providing an efficient and simple way to produce gas-phase $[M–H]^-$ ions. Highly informative negative ions MS/MS spectra showing several diagnostic fragment ions were obtained, mainly A-type cross-ring and C-type glycosidic cleavages. Indeed, cross-ring cleavages of monosaccharides with formation of $^{0,2}A$, $^{0,3}A$, $^{2,4}A$, $^{2,5}A$, $^{3,5}A$ and $^{0,3}X$ product ions dominate the MS/MS spectra. A significant difference between reducing (e.g., lactose, maltose) and non-reducing disaccharides (e.g., sucrose, trehalose) was observed. Though disaccharides with the anomeric positions blocked give rise to deprotonated molecules, $[M–H]^-$, at *m/z* 341.1, reducing ones exhibited a peak at *m/z* 340.1, most likely as radical anion, $[M–H^{\bullet}–H]^{-\bullet}$. The superiority of TPPN was clearly demonstrated by comparison with well recognized matrices, such as 2,5-dihydroxybenzoic acid and 2',4',6'-trihydroxyacetophenone (positive ion mode) and *nor*-harman (negative ion mode). MALDI MS/MS experiments on isotopically labeled sugars have greatly supported the interpretation of plausible fragmentation pathways.

1. INTRODUCTION

Matrix-assisted laser desorption/ionization mass spectrometry (MALDI-MS) is largely used to analyze biological molecules such as proteins, peptides, polymers, lipids and carbohydrates [1–3]. Carbohydrates, abundant in living organisms, are involved in many biological processes, such as immune responses, cell communication and molecular recognition [4–6]. Sucrose, for instance, is an essential biomarker for assessing sugar uptake associated with several diseases such as metabolic syndrome, obesity, and cardiovascular problems [7].

Although MALDI MS has been recognized as a potentially useful technique for saccharides and glycans [8–10], some analytical challenges, dictated by their inherently low ionization efficiency, are still to be faced. Neutral oligosaccharides are usually observed as alkali ion adducts in positive ion mode using either conventional matrices, such as 2,5-dihydrobenzoic acid (DHB) [11] and 2',4',6'-trihydroxyacetophenone (THAP) [12], or alternative matrices, such as gold nanoparticles [13], carbon nanotubes [14, 15], quantum dots [16] and ionic liquids [17]. Although the coordination to alkali metal cations stabilizes the carbohydrate adducts in the gas-phase, it drives the fragmentation processes preferentially towards ring-ring cleavage thus limiting sequence information [18]. Indeed, positive ion spectra are dominated by glycosidic cleavage ions most of which formed by unspecific, multiple pathways [19], leading to ambiguous structural characterization. Conversely, negative ion mass spectra tend to be much more informative as a result of predominant cross-ring cleavage ions [20, 21] as demonstrated, for example, by negative-ion electrospray ionization (ESI) MS of milk oligosaccharides [22]. Unfortunately, negative-ion MALDI MS is *de facto* limited to acidic oligosaccharides [23, 24] due to the inability to produce deprotonated molecules ($[M–H]^-$) in the gas-phase from neutral sugars. To overcome this drawback, the formation of stable anionic adducts employing conventional MALDI matrices mixed with e.g.

chloride salts [25], sulphuric acid [26][27], and benzenesulfonic/*p*-toluenesulfonic acids [28] has been proposed. These adducts are not always useful for neutral sugar fragmentation studies because the predominant product ion is mainly the dissociated anion of the used acid. Alternatively, negative ions can be produced by chemical derivatization of saccharides using 2-aminobenzoic acid [29] or 2-aminoacridone [30]; however, the negative charge tends to be located on the acidic moiety of the derivatized compounds, thus hindering the abstraction of hydroxyl protons, a condition strictly required to generate diagnostic product ions. Other derivatizing agents, such as aminonaphthalene sulfonic acids [31], used to negatively charge neutral saccharides for capillary electrophoresis separation, have not been investigated in the framework of MALDI MS.

A further approach to enhance the ionization of neutral saccharides in negative-ion mode MALDI MS is represented by the use of non-conventional matrices [32]. Nonami *et al.* proposed *nor*-harman (i.e., a β-carboline alkaloid) as a matrix for negative ion MALDI MS of neutral cyclomalto-oligosaccharides [33]; however, the extension to linear oligosaccharides revealed unsuccessful since the resulting deprotonated molecules were unstable [34]. Some improvements were reported by Wong *et al.* [28] using *nor*-harman in the presence of diluted sulfuric acid; apparently, formation of HSO_4^- anionic adducts occurred only for oligosaccharides containing at least four monomer units, with sulfation occurring at higher laser energy. A more effective approach was reported by Cole and coworkers [35] using harmine (again a β-carboline alkaloid derivative) matrix doped with ammonium chloride. By this method, small molecules including sucrose and cyclodextrins were characterized. Yet, due to the presence of chlorine isotopes and abundant matrix-related cluster ions, the generated mass spectra are difficult to interpret, especially in the case of oligosaccharide mixtures. Thus, devising an efficient MALDI matrix capable of producing deprotonated molecules of diverse

neutral saccharides is still an open challenge. Potentially, a proton sponge as 1,8-bis(dimethylamino)naphthalene (DMAN) proposed by Svatos' group [36] could be effective for the analysis of these compounds for the analysis of these compounds; unfortunately, DMAN suffers from poor stability (i.e. high sublimation rate) under high vacuum conditions which led to variable matrix-to-analyte ratio and contamination of the ion optics of the mass spectrometer [37]. Indeed, 1,8-di(piperidinyl)-naphthalene was alternatively proposed by the same group as deprotonating matrix for glucose detection in negative ion mode MALDI MS [38].

A new class of superbasic proton sponges, easily synthesised *via* a Kirsanov condensation, based on the 1,8-bisphosphazenylnaphthalene (PN) motif, and displaying pK_{BH+} values around 30 (in acetonitrile) has been characterised and described [39]. The use of 1,8-bis(trispyrrolidinylphosphazenyl)naphthalene (TPPN) as MALDI matrix for hardly ionizable low-molecular weight compounds was recently reported [40]. TPPN can deprotonate compounds such as sterols, steroids and fatty alcohols in the condensed phase (before laser irradiation) according to a mechanistic model known as matrix assisted ionization/laser desorption. TPPN should be potentially able to deprotonate neutral saccharides as well, as evidenced by some preliminary experiments showing that, indeed, the $[M–H]^-$ ion of sucrose could be detected at *m/z* 341.110 [40]. Here, we report the use of TPPN matrix for negative ion MALDI-MS and MS/MS analysis of mono- and di-saccharides, cyclodextrins and saccharide alditols. The MS/MS spectra of precursor ions showed several product ions, mainly due to cross-ring and C-type glycosidic cleavages, which allow to attain significant structural information. Moreover, ^{13}C labeled fructose and glucose were also analyzed by MALDI MS/MS aiming to propose a plausible fragmentation pathway.

2. MATERIALS AND METHODS

2.1 Chemicals. Water, acetonitrile, methanol, 2,5-dihydroxybenzoic acid (DHB), 2',4',6'-trihydroxyacetophenone (THAP), *nor*-harman, trifluoroacetic acid (TFA), ammonium chloride, D-glucose, D-galactose, D-fructose, D-mannose, sucrose, gentiobiose, trehalose, lactose, lactulose, raffinose, stachyose, α- and β-cyclodextrin, D-glucose-1,2-^{13}C, D-fructose-1-^{13}C were obtained from Sigma-Aldrich (Milan, Italy). TPPN was *in house* synthesized following a reported protocol [29]. Cow milk, soy drink and sugar-free chewing gum were purchased from a local supermarket. All solvents used were LC–MS grade. Mass standards kit for calibration was purchased from AB Sciex (Ontario, Canada).

2.2 Instrumentation. All experiments were performed using a 5800 MALDI ToF/ToF analyzer (AB SCIEX, Darmstadt, Germany) equipped with a neodymium-doped yttrium lithium fluoride (Nd:YLF) laser (345 nm), in reflectron positive and negative mode with a typical mass accuracy of ≤10 ppm. At least 6×1000 laser shots were typically accumulated in MS mode by a random rastering pattern, using a laser pulse rate of 400 Hz, whereas in MS/MS mode up to 8×1000 laser shots were acquired (at a pulse rate of 1000 Hz) and averaged. Laser fluences of 2.5–2.7 J/m^2 were typically used. MS/MS experiments were performed setting a potential difference between the source and the collision cell of 1 kV; ambient air or Argon (typical pressure of 10^{-6} Torr) were used as the collision gas. The delayed extraction (DE) time was set at 240 ns. DataExplorer software 4.0 (AB Sciex) was used to control the acquisitions and to perform the initial elaboration of data while SigmaPlot 11.0 was used to graph final mass spectra. ChemDraw Pro 8.0.3 (CambridgeSoft Corporation, Cambridge, MA, USA) was employed to draw chemical structures.

2.3 Sample Preparation.

DHB matrix solution was typically prepared at a concentration of 10 mg/mL in a 70:30

acetonitrile/water solution containing 0.1% TFA. THAP was prepared in acetonitrile (10 mg/mL) and then mixed with 10% NaCl solution (3:1, v:v). *Nor*-harman was dissolved in acetonitrile (10 mg/mL) and then mixed 1:1 (v:v) with NH_4Cl solution (10 mg/mL). Finally, TPPN solution was prepared at 6 mg/mL concentration in acetonitrile. Saccharide standards were dissolved in ultrapure water to a concentration of 5 mM. Sucrose solutions at decreasing concentration (down to 10^{-7} mol/L) were used for the sensitivity tests. Milk and soy drink were simply diluted in water (1:10) while sugar free chewing gum sample was crushed and 1 mg dissolved in 1 mL of water.

2.4 MALDI MS analysis. For MALDI analysis, usually 5 µL of standard saccharides or real samples solution were mixed with each matrix (1:1 or 2:1, v/v ratio). 1 µL of the analyte-matrix mixture was spotted directly on the target plate, dried in the dark and analysed. Unless otherwise specified the dried-droplet method was thoroughly used in this work.

3. RESULTS AND DISCUSSION

3.1 MALDI MS of monosaccharides

MALDI mass spectra of D-galactopyranose (A), β-D-fructopyranose (B), D-glucopyranose, (C) and D-mannopyranose (D) obtained using TPPN as matrix, are shown in Figure 1. All these monohexoses exhibit a base peak due to deprotonated molecules ($[M–H]^-$) at *m/z* 179.148; the occurrence of a peak at *m/z* 178.047 is also clearly seen, thus suggesting the concurrent formation of a $[M–2H]^{-\bullet}$ radical anion, a feature also shared by reducing disaccharides (*vide infra*). Other signals at *m/z* 71.014, 89.024, 101.017, 225.073, 251.077, 269.087, and 281.087 were detected with variable intensities. It is known that under high-pH conditions as those present in the sample spot, sugars undergo retro-aldolization reactions, yielding stable α-dicarbonyl compounds as glyoxal, methylglyoxal, glycolaldehyde, 1-deoxyglucosone, 3-

deoxyglucosone, butanedione, and other derivatives [41–44]. Thus, the peak signals in the low *m/z* range (i.e., *m/z* 71.014, 89.024 and 101.017) are likely attributable to monohexose's deprotonated by-products (pre-formed in the condensed phase as expected for a MAILD matrix), namely: 3-oxoprop-1-en-2-olate ($[C_3H_4O_2–H]^–$, monoisotopic mass 71.0139), 2-hydroxypropanoate or lactate anion ($[C_3H_6O_3–H]^–$, monoisotopic mass 89.0244) and 2-oxobutanoate ($[C_4H_6O_3–H]^–$, monoisotopic mass 101.0244), respectively. These assignments were supported by high-energy collision-induced dissociation tandem mass spectrometry (CID-MS/MS); as an example, Fig. S1 (Supplemental information) reports the product ion spectra of precursor ions at *m/z* 101.03 and 71.03, plots A and B, respectively.

Interestingly, tandem MS analyses of ions at higher *m/z* values exhibited a characteristic behaviour. For instance, the peak at *m/z* 281 generated a MS/MS spectrum (see Fig. S2A) featuring two main product ions at *m/z* 101.03 and 179.15. Similar findings were obtained for the precursor ion at *m/z* 251, which originated product ions at *m/z* 71.01 and 179.15 (see Fig. S2B). In the case of precursor ions at *m/z* 225 and 269, product ions at *m/z* 45.01 and 179.15, and at *m/z* 89.02 and 179.15, respectively, were observed suggesting the formation of adducts between monohexoses and the already mentioned by-products formed in the sample spot. Thus, the peak at *m/z* 251.08 may be due to a deprotonated adduct $[C_9H_{16}O_8–H]^–$ formed between a hexose and 3-oxoprop-1-en-2-olate. Likewise, the peak at *m/z* 281.09 $[C_{10}H_{18}O_9–H]^–$ likely mirrors an adduct formation between a hexose and 2-oxobutanoate ion, whereas the peak at *m/z* 269.09 $[C_9H_{18}O_9–H]^–$ could be due to an adduct formation with a lactate ion. Finally, the peak at *m/z* 225.06 $[C_{10}H_{18}O_9–H]^–$ is most likely an adduct with a formate ion ($[CH_2O_2–H]^–$, monoisotopic mass 44.9982). Further support to this suggestion is given by the observation that the signal intensities of these adducts increased on increasing the sugar amount on the spot (up to three times).

The deprotonated molecule of each sugar was isolated (±3 *m/z* units) and CID-MS/MS was accomplished; ^{13}C labelled monosaccharides were also investigated to elucidate the fragmentation pattern. The CID-MS/MS spectra of fructose (A) and $^{13}C_1$ labelled fructose (B) are shown in Figure 2. Spectrum in Figure 2A, clearly suggests that the observed product ions are mainly formed by the loss of one or two water molecules (e.g. signals at *m/z* 161.04 and 143.04), by formaldehyde loss (e.g. ion at *m/z* 149.04) and by cross-ring cleavages or combinations of these neutral losses (*vide infra*). Whereas water loss ultimately induces the formation of a double-bond, the loss of neutral formaldehyde triggers ring cleavage. Inspection of the spectrum in Figure 2B indicates that many fragments display the $^{13}C_1$ contribution, thus suggesting that at least two different fragmentation pathways are possible. According to the nomenclature of Domon and Costello [45] most product ions can be explained by considering the formation of X/A ions at different ring positions; for instance, the formation of *m/z* 119.03 is due to either 0,1 or 3,4 ring cleavage. **Scheme 1** summarizes the production of $^{0,2}A$, $^{2,4}A$, $^{2,5}A$, $^{3,4}A$ and $^{0,2}X$, cross-ring cleavages from deprotonated molecules. Interestingly, the ion at *m/z* 101.02 suggests that only the fragment including the labelled carbon is formed; this product ion, never reported in previous studies on monosaccharides, was detected as radical anion also in non-labelled fructose at *m/z* 100.02 (see plot 2A). Comparing this outcome with that obtained by ESI-MS/MS [46] an overlap of all the fragments was noticed except for this last product ion, thus suggesting that its formation is favoured during MALDI-MS/MS likely due to a different energy regimen in the high-energy CID. Worth of note is also the peak at *m/z* 108.03 in labelled fructose which can be generated only following an interconversion to the fructopyranose form. To confirm these suggestions, glucose labelled with two ^{13}C was investigated. Figure 3 shows CID-MS/MS product ion spectra of glucose (A) and glucose labelled as $^{13}C_{1,2}$ (B). Many product ions of glucose (plot A) overlaps

those observed for fructose (see plot A in Figure 2) with only minor differences in relative intensities. MS/MS spectrum of labelled glucose exhibits two well-defined components signifying the concomitant occurrence of two cross ring cleavages. Once again, the peak at *m/z* 102.09 was observed as radical anion free from the isotope contribution, confirming the distinctive formation of the fragment with labelled carbon. **Scheme 2** reports the suggested assignments as product ions of signals detected in Figure 3. Additional examples (see Fig. S3) of galactose (A) and mannose (B) MS/MS spectra are also given for comparison. Once again, the main product ions are explained as water or formaldehyde loss, cross-ring cleavages and combinations of these processes resulting in close-related spectra of fructose and glucose (see Scheme 1). Overall, the product ion mass spectra of the investigated monohexoses are not easily distinguishable. The key differences are found in the signal intensities of peaks at *m/z* 119 and *m/z* 107 probably suggesting competing fragmentation processes i.e. the loss of two formaldehyde molecules (CH_2O), preferred in deprotonated galactose and mannose, and the neutral loss of $C_3H_4O_2$, most likely methylglyoxal, preferred in deprotonated fructose and glucose.

Negative ion MALDI mass spectra of fructose, glucose, galactose and mannose acquired using a *nor*-harman matrix containing NH_4Cl, showed their respective chloride adduct at *m/z* 214.99. MS/MS spectra of this precursor ion (see Fig. S4) showed a base peak at *m/z* 34.97 (chloride ion) and a small contribution from the deprotonated sugar at *m/z* 179.14. Noticeably, such a limited fragmentation precludes the structural characterization of monosaccharides. The same findings were obtained when analysing sugars in positive ion mode by using THAP or DHB matrices. Here, isolating the sodium adduct for each sugar at *m/z* 203, the resulting MS/MS spectra were dominated by the sodium ion at *m/z* 23.00 together with two other ions at *m/z* 58.06 and 102.08 (see Fig. S5). The last ion may be due to the

radical cation $C_4H_6O_3^{+\bullet}$ generated after the loss of water and two formaldehyde molecules; apparently, this ion generates that at *m/z* 58.06 after CO_2 loss.

3.2 Saccharide alditols

Negative ion MALDI MS experiments (TPPN as the matrix) on xylitol ($C_5H_{12}O_5$), sorbitol ($C_6H_{14}O_6$), mannitol ($C_6H_{14}O_6$), isomalt (1-O-α-D-glucopyranosyl-D-mannitol ($C_{12}H_{24}O_{11}$), monoisotopic mass 344.13 Da), lactitol (4-O-β-D-glucopyranosyl-D-glucitol, $C_{12}H_{24}O_{11}$), and maltitol (4-O-α-glucopyranosyl-D-sorbitol, $C_{12}H_{24}O_{11}$) were performed. Product ion mass spectra of sorbitol (A), mannitol (B), and maltitol (C) are reported in Figure 4 and product ions summarized in Table 1 along with the most likely assignment and abundances normalized to the base peak, viz. *m/z* 89.02 for sorbitol, *m/z* 119.03 for mannitol and *m/z* 179.14 for maltitol. As expected the MS/MS spectra of sorbitol and mannitol were somewhat similar (see plots A and B of Figure 4), though a different fragmentation pattern was observed for maltitol, which is a disaccharide alditol. Most of the observed peaks are shared with the corresponding monosaccharide with different relative intensities. A deeper inspection reveals some diagnostic ions at *m/z* 163.07, 159.06, 115.03, 103.03, 73.03 and 59.02 for sorbitol/mannitol and at *m/z* 283.07 and 59.08 for maltitol. An interesting issue is the ability to provide a rapid screening of alditols in a sugar-free chewing gum, as reported in Fig. S6 and Table S1. These results demonstrate the possibility of widening the use of TPPN as deprotonating matrix, thus representing the first report on the negative ion MALDI MS/MS of saccharide alditols.

3.3 Disaccharides

A different ionization behavior was observed for reducing (i.e., lactose, maltose, lactulose and gentobiose) and non-reducing (i.e., sucrose, trehalose) disaccharides, ($C_{12}H_{22}O_{11}$). Indeed,

sucrose (O-α-D-glucopyranosyl-(1→2)-β-D-fructofuranoside) and trehalose (α-D-glucopyranosyl-(1→1)-α-D-glucopyranoside) were detected as $[M-H]^-$ ion at *m/z* 341.108 while reducing sugars were observed at *m/z* 340.102 likely as $[M-2H]^{-\bullet}$ (not shown). The inspection of the isotopic pattern of deprotonated reducing sugars, revealed that the M+1 isotope exhibited a relative abundance around 23-25%, which was higher than the expected natural isotopic abundance (ca. 14%), thus suggesting a small contribution of the deprotonated molecule $[M-H]^-$. The leading formation of the radical anion could be somehow related to the different structure of reducing sugars. Indeed, while non-reducing disaccharides are stuck in the cyclic form, reducing disaccharides can be converted into an open-chain form holding an aldehyde moiety. This type of isomerization is catalysed by bases or acids [47]. Therefore, compared to non-reducing sugars, the proton in *α* position can be lost more easily in the condensed phase due to the interactions with the strong base TPPN, giving rise to an aldo-enol stabilized by resonance (**Scheme 3**). Likely, during the laser irradiation reducing sugars may loss another hydrogen as a radical ($H^\bullet$) in the gas phase (probably from the hydroxyl residues or from aldehyde, see pathways **a** and **b** in Scheme 3) generating the radical anion $[M-H^\bullet-H]^{-\bullet}$ also stabilized by resonance. An indirect support to this hypothesis is given by retinaldehyde (3,7-dimethyl-9-(2,6,6-trimethylcyclohexen-1-yl)nona-2,4,6,8-tetraenal) spectrum that exhibits a deprotonated molecule $[M-H]^-$ at *m/z* 283.207 along with a radical anion $[M-2H]^{-\bullet}$ at *m/z* 282.199 (data not shown), originating through the aldehyde proton loss as radical during the desorption/ionization process. Apart from mechanistic considerations, this different behavior allows to easily distinguish between reducing and non-reducing sugars in MS mode. Figure 5 shows the MALDI-MS/MS product ion spectra of deprotonated sucrose at *m/z* 341, lactose at *m/z* 340 and maltose at *m/z* 340, plots (A), (B) and (C), respectively. The tandem MS spectrum of a non-reducing sugar (sucrose) is dominated by a product ion at *m/z*

179.14 observed in all disaccharides and formed through glycoside bond cleavage. On the contrary, the mass spectra of lactose (B) and maltose (C), almost identical each other, are dominated by two fragment ions at *m/z* 322.09 (loss of a water molecule) and 262.07 (combined loss of H_2O and two formaldehyde molecules) that were not observed for sucrose. Though with different intensities, the peak at *m/z* 281.09 was common to all investigated sugars, while the peak at *m/z* 295.10 (loss of a formate radical, $HCOO^{\bullet}$) was detected only in deprotonated lactose (see plot B). Moreover, a distinguishing feature of reducing saccharides was the presence of a fragment at *m/z* 159.04 which could correspond to a dehydrated monosaccharide residue $[C_6H_7O_5]^-$. The other common peaks at *m/z* 161.05, 119.03, 107.03, 89.03 can be explained looking at Schemes 1 and 2. The same fragmentation pattern was observed also by analyzing two real samples. Fig. S7 reports MALDI MS/MS spectra of sucrose from soy drink at *m/z* 341 (A) and lactose in bovine milk at *m/z* 340 (B). Likewise, samples containing gentobiose, lactulose and trehalose were investigated (data not shown). An additional proof of the performance of the TPPN matrix was provided selecting sucrose as model sugar (Fig. S8). Sucrose was also investigated in negative ion mode by using a *nor*-harman as a matrix. Each carbohydrate detected as chloride adduct (i.e., $[M+Cl]^-$) at *m/z* 377.10 was isolated and fragmented (Fig. S9). As for monosaccharides, the base peak was represented by the chloride ion at *m/z* 34.97 though other low intensity ions were detected with some differences among reducing and non-reducing sugars. The main product ions of the sucrose adduct (Fig. S9A) were represented by peaks at *m/z* 341.16 (deprotonated sucrose), *m/z* 215.08 and *m/z* 59.01 ($[C_2H_3O_2]^-$, see Scheme 1). This last peak was also observed in the lactose MS/MS spectrum (Fig. S9B) together with those at *m/z* 179.15 and 161.06 both generated from glycosidic bond cleavage. So, also for disaccharides the tandem mass spectra of chloride adducts appear less informative compared to the ones acquired using TPPN as a

matrix. The same remark applies to positive ion mode MALDI MS/MS of these sugars using THAP or DHB as matrices (Fig. S10). The sodiated adducts at *m/z* 365 produced main product ions at *m/z* 203.05 and 185.04 (corresponding to sodiated and protonated adducts, respectively, formed by glycosidic bond cleavage), *m/z* 305.07 (loss of two formaldehyde molecules) and *m/z* 23.00 (Na^+ ion).

3.4. Tri- and tetra-saccharides

Raffinose is a non-reducing sugar composed of a galactose (Gal) unit linked to the glucose moiety of sucrose via α-(1→6) glycosidic linkage. The base peak in the MALDI spectrum, corresponding to deprotonated raffinose $[M-H]^-$ at *m/z* 503, was isolated as precursor ion and fragmented (Figure 6A). The peaks at *m/z* 341.11 and 179.14 correspond to glycosidic cleavage products C_2 and C_1 [45] formed by the loss of two and one hexose moieties, respectively, while the peaks at *m/z* 323.10 and 161.05 are the corresponding B_2 and B_1 type ions (loss of water). Multiple cross-ring cleavages generated A type ions at *m/z* 281.08 ($^{0,2}A_2$), 251.07 ($^{0,3}A_2$), 221.06 ($^{0,4}A_2$), 119.05 ($^{0,2}A_1$), 101.15 ($^{2,5}A_1$) and 89.05 ($^{0,2}A_1$), where superscripts indicate the position of the cross-ring cleavage. Such linkage-specific cross-ring fragmentations have already been described in negative-ion low-energy collision activation Fourier-transform mass spectrometry (FT-MS) [48] and in CID experiments by ESI-ion trap MS [49].

Stachyose is a tetrasaccharide naturally occurring in numerous vegetables, beans and plants, consisting of two α-galactose units, one α-glucose unit, and one β-fructose unit sequentially linked as gal(α1→6)gal(α1→6)glc(α1→2β)fru. The base peak in the MALDI spectrum, corresponding to deprotonated stachyose $[M-H]^-$ at *m/z* 665, was isolated and fragmented (Figure 6B). The peaks at *m/z* 503.09, 341.09 and 179.14 are assigned to the main glycosidic cleavage products C_3, C_2 and C_1 formed *via* the neutral loss of one, two and three

hexose moieties, respectively; peaks at *m/z* 485.07, 323.10 and 161.05 are the corresponding B_3, B_2 and B_1 ions (loss of water from C_n ions). The multiple cross-ring cleavages are observed to form A-type ions at *m/z* 443.06 ($^{0,2}A_3$), 425.05 ($^{2,5}A_3$), 413.06 ($^{0,3}A_3$), 383.05 ($^{0,4}A_3$), 281.04 ($^{0,2}A_2$), 251.04 ($^{0,3}A_2$), 221.04 ($^{0,4}A_2$), and 101.10 ($^{2,5}A_1$).

The same tetrasaccharide was examined in positive ion mode by using DHB as the matrix. The sodiated adduct at *m/z* 689 was isolated and fragmented (data not shown) generating a very intense ion at *m/z* 527 (corresponding to sodiated glycosidic cleavage product C_3) together with sodiated B_3 at *m/z* 509 (loss of H_2O from C_3) and low intensity fragments at *m/z* 365 and 203 (sodiated C_2 and C_1, respectively) and *m/z* 347 and 185 (sodiated B_2 and B_1, respectively). Again, no information about cross-ring cleavages could be gained.

3.5. Cyclodextrins

Finally, cyclic oligosaccharides such as cyclohexaamylose and cycloheptaamylose also known as α- and β-cyclodextrins (CDs) were considered. Post-source decay (PSD) spectra in negative ion mode MALDI-MS of αCD and ϒCD (i.e., cyclooctaamylose) are described in literature [34]. In the case of deprotonated α-CD ($[C_{36}H_{59}O_{30}]^-$, *m/z* 971.31), product ions were detected at *m/z* 851, 689, 527 spaced by 162 Da, corresponding to the neutral loss of glucose residues. Notably, the base peak in the PSD spectrum was at *m/z* 851 with a difference of 120 Da from the precursor ion due to the neutral loss of $C_4H_8O_4$, as a result of a cross-ring fragmentation [24]. We also detected cross-ring fragments at *m/z* 851.27 and 1013.30 for α-CD and β-CD, respectively (plots A and B of Figure 7). Moreover, looking at α-CD spectrum in plot A, peak signal at *m/z* 689.23, 527.19, 365.12 and 203.08 are observed all originating from the product ion at *m/z* 851.27 through glycosidic bond cleavages and subsequent loss of the glucose units.

However, many other peaks are detected and some of them have never been described before. So, indicating as R the $C_4H_8O_4$ unit (120 Da), G the glucose unit (162 Da) and AH the anhydro hexose unit (144 Da) it is possible to explain all product ions observed in the spectrum from glycosidic bond and cross-ring cleavages as reported in the Supplementary Material. ~~follows: $[\alpha CD-2R-H]^-$ (731.24), $[\alpha CD-R-AH-H]^-$ (707.24), $[\alpha CD-R-G-H]^-$ (689.23), $[\alpha CD-2R-AH-H]^-$ (587.21), $[\alpha CD-2R-G-H]^-$ (569.20), $[\alpha CD-R-G-AH-H]^-$ (545.19), $[\alpha CD-R-2G-H]^-$ (527.19), $[\alpha CD-3G-H]^-$ (485.18), $[\alpha CD-2R-2AH-H]^-$ (443.16), $[\alpha CD-2R-G-AH-H]^-$ (425.16), $[\alpha CD-2R-2G-H]^-$ (407.13), $[\alpha CD-R-2G-AH-H]^-$ (383.14), $[\alpha CD-R-3G-H]^-$ (365.12), $[\alpha CD-3G-AH-H]^-$ (341.12), $[\alpha CD-4G-H]^-$ (323.12), $[\alpha CD-2R-G-2AH-H]^-$ (281.10), $[\alpha CD-2R-2G-AH-H]^-$ (263.08), $[\alpha CD-5G-H]^-$ or $[G-H]^-$ (161.06) and $[AH-H]^-$ (143.05). The tandem mass spectrum of $[\beta CD-H]^-$ (*m/z* 1133), shown in plot B, reveals the same fragmentation pathway as $[\alpha CD-H]^-$.~~

When α-CD was analyzed and fragmented in positive ion mode as sodiated adduct $[\alpha CD+Na]^+$ at *m/z* 995 (plot C of Figure 7), few product ions were detected at *m/z* 833.25, 671.20, 509.15, 347.11, 185.06 with a delta mass of 162 Da, corresponding to the loss of glucose units. Similar fragmentation pattern was experienced for β-CD (Figure 7D). Likewise, mass spectra of cyclic oligosaccharides in positive ion mode revealed very limited information since cross-ring cleavages are absent.

4. CONCLUSIONS

It is demonstrated, for the first time, that TPPN can be successfully used as a matrix for an in-depth characterization of neutral saccharides by means of MALDI–MS/MS. TPPN is able to ionize such sugar compounds by abstracting very weakly acidic protons and favoring the formation of intact deprotonated molecules without the use of any other additive or co-

matrix. Compared with other employed matrices such as DHB, THAP, and *nor*-harman, TPPN exhibited better spectral quality, lower matrix related background, improved signal-to-noise ratio and extended fragmentation, thus allowing to gather more structural information. Besides the conventional even-electron anion ($[M–H]^-$), reducing disaccharides exhibited a peak signal as radical anion, $[M–H^{\bullet}–H]^{-\bullet}$, thus affecting the resulting tandem MS spectra. Likely, molecular dynamics simulations would be useful to provide clues to understanding the ionization mechanism of neutral saccharides along with radial anion formation. TPPN matrix was successfully applied for the analysis of neutral sugars also in food samples as bovine milk and soy drink. The results allowed us to speculate that TPPN could be a useful matrix for MALDI MS/MS of oligosaccharide mixtures and could open prospects for its application also on complex biological samples.

ACKNOWLEDGMENTS

This work was supported by the project PONa3_00395/1 “BIOSCIENZE & SALUTE (B&H)” of Italian Ministero per l'Istruzione, l'Università e la Ricerca (MIUR). Dr. Costantino Chiapperino is acknowledged for his help in running some MALDI experiments.

REFERENCES

1. Hillenkamp, F., Katalinic, J.P.: MALDI MS A Practical Guide to Intrumentation, Methods and Applications. Wiley-VCH Verlag, Weinheim, Germany. (2007).

2. Webster, J., Oxley, D.: Protein identification by MALDI-TOF mass spectrometry. Methods in Molecular Biology. 800, 227–240 (2012).

3. Calvano, C.D., Monopoli, A., Ditaranto, N., Palmisano, F.: 1,8-bis(dimethylamino)naphthalene/9-aminoacridine: a new binary matrix for lipid fingerprinting of intact bacteria by matrix assisted laser desorption ionization mass spectrometry. Analytica chimica acta. 798, 56–63 (2013).

4. Sinnott, M., Sinnott, M.: Carbohydrate Chemistry and Biochemistry. Royal Society of Chemistry, Cambridge (2007).

5. Van Hoffen, E., Ruiter, B., Faber, J., M'Rabet, L., Knol, E.F., Stahl, B., Arslanoglu, S., Moro, G., Boehm, G., Garssen, J.: A specific mixture of short-chain galacto-oligosaccharides and long-chain fructo-oligosaccharides induces a beneficial immunoglobulin profile in infants at high risk for allergy. Allergy: European Journal of Allergy and Clinical Immunology. 64, 484–487 (2009).

6. Hassler, C.S.C., Schoemann, V., Nichols, C.M., Butler, E.C.V.E., Boyd, P.W.P., Mancuso Nichols, C., Butler, E.C.V.E., Boyd, P.W.P.: Saccharides enhance iron bioavailability to Southern Ocean phytoplankton. Proceedings of the National Academy of Sciences of the United States of America. 108, 1076–81 (2011).

7. Tasevska, N.: Urinary sugars—a biomarker of total sugars intake. Nutrients. 7, 5816–5833 (2015).

8. Harvey, D.J.: Matrix-assisted laser desorption/ionization mass spectrometry of carbohydrates. Mass Spectrometry Reviews. 18, 349–450 (1999).

9. Domann, P., Spencer, D.I.R., Harvey, D.J.: Production and fragmentation of negative ions from neutral N-linked carbohydrates ionized by matrix-assisted laser desorption/ionization. Rapid Communications in Mass Spectrometry. 26, 469–479 (2012).

10. Kailemia, M.J., Ruhaak, L.R., Lebrilla, C.B., Amster, I.J.: Oligosaccharide Analysis by Mass Spectrometry: A Review of Recent Developments. Analytical Chemistry. 86, 196–212 (2014).

11. Štikarovská, M., Chmelík, J.: Determination of neutral oligosaccharides in vegetables by matrix-assisted laser desorption/ionization mass spectrometry. Analytica Chimica Acta. 520, 47–55 (2004).

12. Hsu, N.-Y., Yang, W.-B., Wong, C.-H., Lee, Y.-C., Lee, R.T., Wang, Y.-S., Chen, C.-H.: Matrix-assisted laser desorption/ionization mass spectrometry of polysaccharides with 2',4',6'-trihydroxyacetophenone as matrix. Rapid Commun. Mass Spectrom. 21, 2137–46 (2007).

13. Su, C.L., Tseng, W.L.: Gold nanoparticles as assisted matrix for determining neutral small carbohydrates through laser desorption/ionization time-of-flight mass spectrometry. Analytical Chemistry. 79, 1626–1633 (2007).

14. Wang, C., Li, J., Yao, S., Guo, Y., Xia, X.: High-sensitivity matrix-assisted laser desorption/ionization Fourier transform mass spectrometry analyses of small carbohydrates and amino acids using oxidized carbon nanotubes prepared by chemical vapor deposition as matrix. Analytica Chimica Acta. 604, 158–164 (2007).

15. Ren, S., Zhang, L., Cheng, Z., Guo, Y.: Immobilized carbon nanotubes as matrix for MALDI-TOF-MS analysis: Applications to neutral small carbohydrates. Journal of the American Society for Mass Spectrometry. 16, 333–339 (2005).

16. Bibi, A., Ju, H.: Quantum dots assisted laser desorption/ionization mass spectrometric detection of carbohydrates: qualitative and quantitative analysis. Journal of Mass Spectrometry. 51, 291–297 (2016).

17. Fukuyama, Y., Nakaya, S., Yamazaki, Y., Tanaka, K.: Ionic liquid matrixes optimized for MALDI-MS of sulfated/sialylated/neutral oligosaccharides and glycopeptides. Analytical Chemistry. 80, 2171–2179 (2008).

18. Cancilla, M.T., Penn, S.G., Carroll, J.A., Lebrilla, C.B.: Coordination of alkali metals to oligosaccharides dictates fragmentation behavior in matrix assisted laser desorption ionization/Fourier transform mass spectrometry. Journal of the American Chemical Society. 118, 6736–6745 (1996).

19. Harvey, D.J., Martin, R.L., Jackson, K.A., Sutton, C.W.: Fragmentation of N-linked glycans with a matrix-assisted laser desorption/ionization ion trap time-of-flight mass spectrometer. Rapid Commun. Mass Spectrom. 18, 2997–3007 (2004).

20. Chai, W., Lawson, A.M., Piskarev, V.: Branching pattern and sequence analysis of underivatized oligosaccharides by combined MS/MS of singly and doubly charged molecular ions in negative-ion electrospray mass spectrometry. Journal of the American Society for Mass Spectrometry. 13, 670–679 (2002).

21. Harvey, D.J., Royle, L., Radcliffe, C.M., Rudd, P.M., Dwek, R.A.: Structural and quantitative analysis of N-linked glycans by matrix-assisted laser desorption ionization and negative ion nanospray mass spectrometry. Analytical Biochemistry. 376, 44–60 (2008).

22. Pfenninger, A., Karas, M., Finke, B., Stahl, B.: Structural analysis of underivatized neutral human milk oligosaccharides in the negative ion mode by nano-electrospray MSn (Part 2: Application to isomeric mixtures). Journal of the American Society for Mass Spectrometry. 13, 1341–1348 (2002).

23. Papac, D.I., Wong, A., Jones, a J.: Analysis of acidic oligosaccharides and glycopeptides by matrix-assisted laser desorption/ionization time-of-flight mass spectrometry. Analytical Chemistry. 68, 3215–23 (1996).

24. Jacobs, A., Dahlman, O.: Enhancement of the quality of MALDI mass spectra of highly acidic oligosaccharides by using a nafion-coated probe. Analytical chemistry. 73, 405–10 (2001).

25. Breuker, K., Knochenmuss, R., Zenobi, R.: Matrix-assisted laser desorption/chemical ionization with reagent ion generation directly from a liquid matrix. International Journal of Mass Spectrometry. 176, 149–159 (1998).

26. Anissa W. Wong, Mark T. Cancilla, Lisa R. Voss, A., Lebrilla, C.B.: Anion Dopant for

Oligosaccharides in Matrix-Assisted Laser Desorption/Ionization Mass Spectrometry. Anal. Chem. 71, 205–211 (1998).

27. Anissa W. Wong, Mark T. Cancilla, Lisa R. Voss, and, Lebrilla*, C.B.: Anion Dopant for Oligosaccharides in Matrix-Assisted Laser Desorption/Ionization Mass Spectrometry. (1998).

28. Wong, A.W., Wang, H., Lebrilla, C.B.: Selection of anionic dopant for quantifying desialylation reactions with MALDI-FTMS. Analytical Chemistry. 72, 1419–1425 (2000).

29. Thaysen-Andersen, M., Mysling, S., Højrup, P.: Site-specific glycoprofiling of N-linked glycopeptides using MALDI-TOF MS: Strong correlation between signal strength and glycoform quantities. Analytical Chemistry. 81, 3933–3943 (2009).

30. North, S., Birrell, H., Camilleri, P.: Positive and negative ion matrix-assisted laser desorption/ionization time-of-flight mass spectrometric analysis of complex glycans released from hen ovalbumin and derivatized with-2-aminoacridone. Rapid Commun. Mass Spectrom. 12, 349–356 (1998).

31. Lamari, F.N., Kuhn, R., Karamanos, N.K.: Derivatization of carbohydrates for chromatographic, electrophoretic and mass spectrometric structure analysis. Journal of Chromatography B: Analytical Technologies in the Biomedical and Life Sciences. 793, 15–36 (2003).

32. Domann, P., Spencer, D.I.R., Harvey, D.J.: Production and fragmentation of negative ions from neutral N-linked carbohydrates ionized by matrix-assisted laser desorption/ionization. Rapid Commun. Mass Spectrom. 26, 469–479 (2012).

33. Nonami, H., Tanaka, K., Fukuyama, Y., Erra-Balsells, R.: β-carboline alkaloids as matrices for UV-matrix-assisted laser desorption/ionization time-of-flight mass spectrometry in positive and negative ion modes. Analysis of proteins of high molecular mass, and of cyclic and acyclic oligosaccharides. Rapid Commun. Mass Spectrom. 12, 285–296 (1998).

34. Yamagaki, T., Nakanishi, H.: Negative-Mode Matrix-Assisted Laser Desorption/Ionization Mass Spectrometry of Maltoheptaose and Cyclomaltooligosaccharides. Journal of the Mass Spectrometry Society of Japan. 50, 204–207 (2002).

35. Cai, Y., Jiang, Y., Cole, R.B.: Anionic adducts of oligosaccharides by matrix-assisted laser desorption/ionization time-of-flight mass spectrometry. Analytical Chemistry. 75, 1638–1644 (2003).

36. Shroff, R., Rulísek, L., Doubsky, J., Svatos, A.: Acid-base-driven matrix-assisted mass spectrometry for targeted metabolomics. Proceedings of the National Academy of Sciences of the United States of America. 106, 10092–6 (2009).

37. Thomas, A., Charbonneau, J.L., Fournaise, E., Chaurand, P.: Sublimation of New Matrix Candidates for High Spatial Resolution Imaging Mass Spectrometry of Lipids: Enhanced Information in Both Positive and Negative Polarities after 1,5-Diaminonapthalene Deposition. Analytical Chemistry. 84, 2048–2054 (2012).

38. Weißflog, J., Svatoš, A.: 1,8-Di(piperidinyl)-naphthalene – rationally designed MAILD/MALDI matrix for metabolomics and imaging mass spectrometry. RSC Adv. 6,

75073–75081 (2016).

39. Kögel, J.F., Xie, X., Baal, E., Gesevičius, D., Oelkers, B., Kovačević, B., Sundermeyer, J.: Superbasic Alkyl-Substituted Bisphosphazene Proton Sponges: Synthesis, Structural Features, Thermodynamic and Kinetic Basicity, Nucleophilicity and Coordination Chemistry. Chemistry - A European Journal. 20, 7670–7685 (2014).
40. Calvano, C.D., Cataldi, T.R.I., Kögel, J.F., Monopoli, A., Palmisano, F., Sundermeyer, J.: Superbasic alkyl-substituted bisphosphazene proton sponges: a new class of deprotonating matrices for negative ion matrix-assisted ionization/laser desorption mass spectrometry of low molecular weight hardly ionizable analytes. Rapid Commun. Mass Spectrom. 30, 1680–1686 (2016).
41. Baker, J.R., Zyzak, D. V, Thoroe, S.R., Baynes, J.W.: Chemistry of the fructosamine assay: D-glucosone is the product of oxidation of Amadori compounds. Clinical Chemistry. 40, 1950–1955 (1994).
42. Wells-Knecht, K.J., Zyzak, D. V, Litchfield, J.E., Thorpe, S.R., Baynes, J.W.: Mechanism of autoxidative glycosylation: identification of glyoxal and arabinose as intermediates in the autoxidative modification of proteins by glucose. Biochemistry. 34, 3702–9 (1995).
43. Thornalley, P.J., Langborg, A., Minhas, H.S.: Formation of glyoxal, methylglyoxal and 3-deoxyglucosone in the glycation of proteins by glucose. Biochemical Journal. 344, 109–116 (1999).
44. Martins, S.I.F.., Marcelis, A.T.., van Boekel, M.A.J..: Kinetic modelling of Amadori N-(1-deoxy-d-fructos-1-yl)-glycine degradation pathways. Part I—Reaction mechanism. Carbohydrate Research. 338, 1651–1663 (2003).
45. Domon, B., Costello, C.E.: A Systematic Nomenclature for Carbohydrate Fragmentations in FAB-MS/MS Spectra of Glycoconjugates. Glycoconjugate J. 5, 397–409 (1988).
46. March, R.E., Stadey, C.J.: A tandem mass spectrometric study of saccharides at high mass resolution. Rapid Communications in Mass Spectrometry. 19, 805–812 (2005).
47. Gounder, R., Davis, M.E.: Monosaccharide and disaccharide isomerization over Lewis acid sites in hydrophobic and hydrophilic molecular sieves. Journal of Catalysis. 308, 176–188 (2013).
48. Carroll, J.A., Willard, D., Lebrilla, C.B.: Energetics of cross-ring cleavages and their relevance to the linkage determination of oligosaccharides. Analytica Chimica Acta. 307, 431–447 (1995).
49. Antonio, C., Larson, T., Gilday, A., Graham, I., Bergström, E., Thomas-Oates, J.: Hydrophilic interaction chromatography/electrospray mass spectrometry analysis of carbohydrate-related metabolites from Arabidopsis thaliana leaf tissue. Rapid Commun. Mass Spectrom. 22, 1399–1407 (2008).

FIGURE CAPTIONS

Figure 1. Negative ion MALDI-ToF mass spectra of (A) D-galactopyranose, (B) β-D-fructopyranose (C) D-glucopyranose, and (D) D-mannopyranose by using a TPPN matrix. The chemical structures are shown in insets.

Figure 2. Negative ion MALDI-ToF/ToF mass spectra of *m/z*= 179 from (A) fructose and *m/z*= 180 from (B) $^{13}C_1$-fructose by using a TPPN matrix.

Figure 3. Negative ion MALDI-ToF/ToF mass spectra of *m/z*= 179 from (A) glucose and *m/z*= 181 from (B) $^{13}C_1$,C_2-glucose by using a TPPN matrix.

Figure 4. Negative ion MALDI-ToF/ToF mass spectra of (A) sorbitol (*m/z*= 181), (B) mannitol (*m/z*= 181) and (C) maltitol (*m/z*= 343) by using a TPPN matrix.

Figure 5. Negative ion MALDI-ToF/ToF mass spectra of (A) sucrose (*m/z*= 341), (B) lactose (*m/z*= 340), and (C) maltose (*m/z*= 340) by using a TPPN matrix.

Figure 6. Negative ion MALDI-ToF/ToF mass spectra of (A) raffinose (*m/z* =503) and (B) stachiose (*m/z*= 665) by using a TPPN matrix.

Figure 7. Negative ion MALDI-ToF/ToF mass spectra of (A) α-cyclodextrin (*m/z*= 971) and (B) β-cyclodextrin (*m/z*= 1133) by using TPPN as a matrix. Positive MALDI-ToF/ToF mass spectra of (C) α-CD as $[M+Na]^+$ (*m/z*=995) and (D) β-CD as $[M+Na]^+$ (*m/z*=1157) by using THAP as a matrix.

Table 1. Relative intensity of product ions of sorbitol (Sor), mannitol (Man) and maltitol (Mal) observed by MALDI MS/MS using TPPN as matrix (see Figure 4).[a]

m/z	**Chemical Formula**	**Relative intensity (%)[b]**		
343.12	$[C_{12}H_{24}O_{11}–H]^-$	-	-	$[Mal – H]^-$
283.07	$[C_{10}H_{20}O_9–H]^-$	-	-	1.9
179.15	$[C_6H_{12}O_6–H]^-$	$[Sor – H]^-$	$[Man – H]^-$	100
163.07	$[C_6H_{12}O_5–H]^-$	43.5	71.4	1.2
161.05	$[C_6H_{10}O_5–H]^-$	5.3	6.8	4.2
149.05	$[C_5H_{10}O_5–H]^-$	28.3	28.9	1.1
131.03	$[C_5H_8O_4–H]^-$	6.2	5.5	-
119.03	$[C_5H_{12}O_3–H]^-$	95.4	100	13.4
115.03	$[C_5H_8O_3–H]^-$	27.6	14.4	-
107.03	n.a.[c]	9.0	9.8	1.2
103.03	$[C_4H_8O_3–H]^-$	11.2	5.01	-
101.02	$[C_4H_6O_3–H]^-$	24.9	22.4	-
89.07	$[C_3H_6O_3–H]^-$	100	96	3.8
85.02	$[C_4H_6O_2–H]^-$	10.1	7.0	-
73.03	$[C_3H_6O_2–H]^-$	26.7	12.4	-
71.02	$[C_3H_4O_2–H]^-$	27.8	22.7	2.0
59.08	$[C_2H_4O_2–H]^-$	44.9	41.3	5.9

[a] Many product ions are due to losses of water and formaldehyde molecules within the alditol linear chains. [b] Abundances normalized to the base peak at *m/z* 89.02 for sorbitol, *m/z* 119.03 for mannitol and *m/z* 179.15 for maltitol. [c] Not assigned.

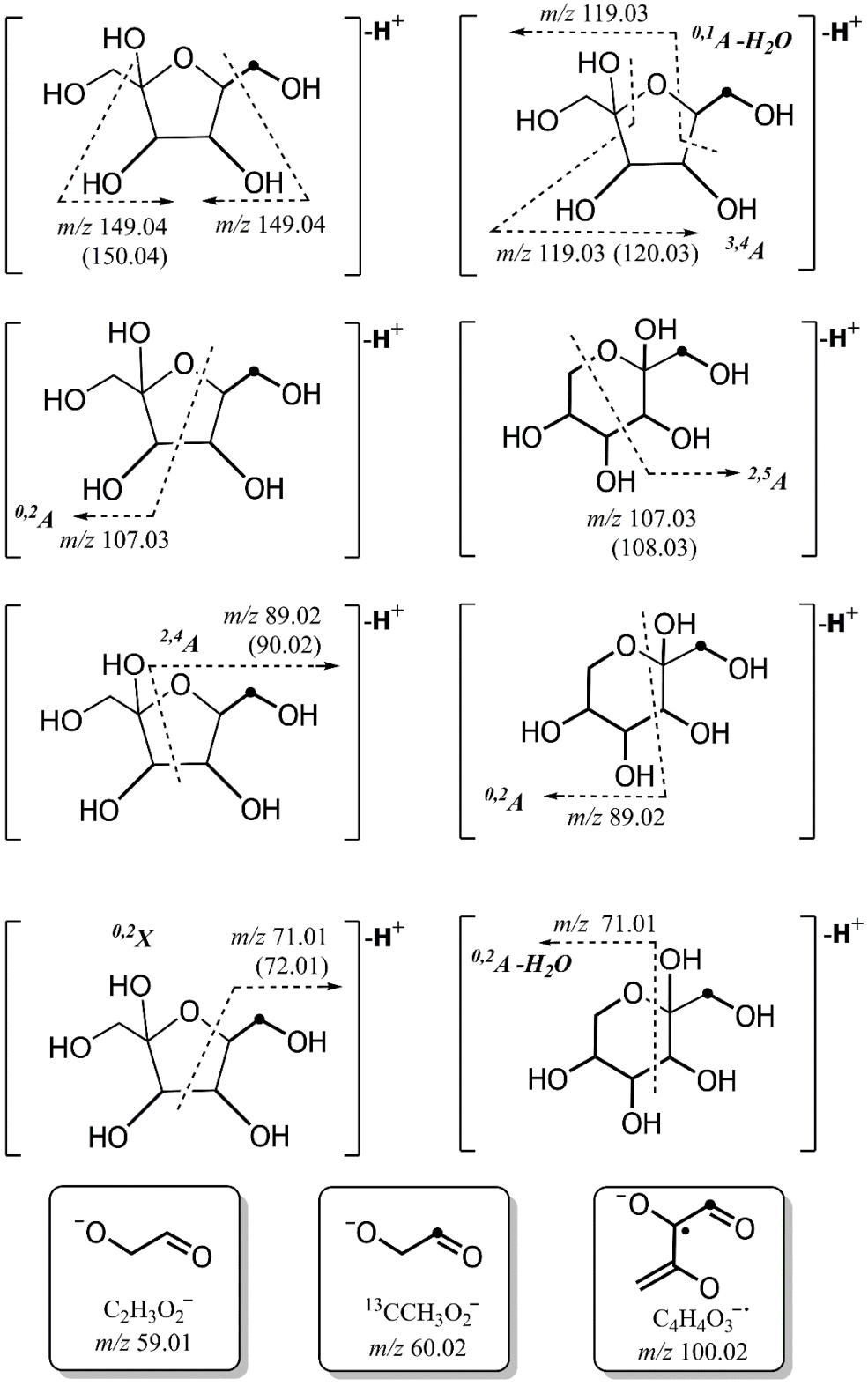

Scheme 1. Suggested cross-ring cleavages of deprotonated fructose identified by MALDI MS/MS using a TPPN matrix. The filled circles represent the labelled isotope of carbon, ^{13}C. The dashed lines identify the broken bonds of the fructose molecule.

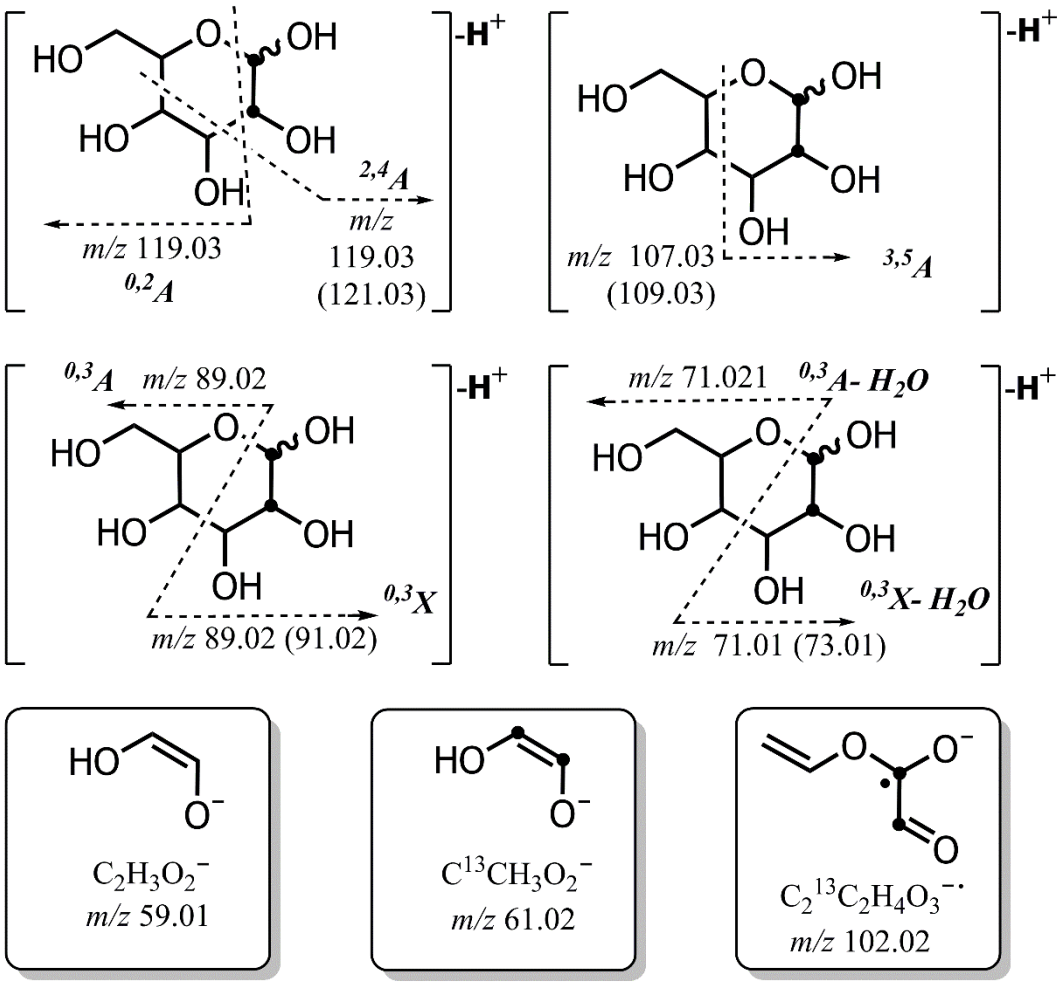

Scheme 2. Suggested cross-ring cleavages of deprotonated glucose identified by MALDI MS/MS using a TPPN matrix. The filled circles represent the heavy isotope of carbon, ^{13}C. The dashed lines identify the broken bonds of the glucose molecule.

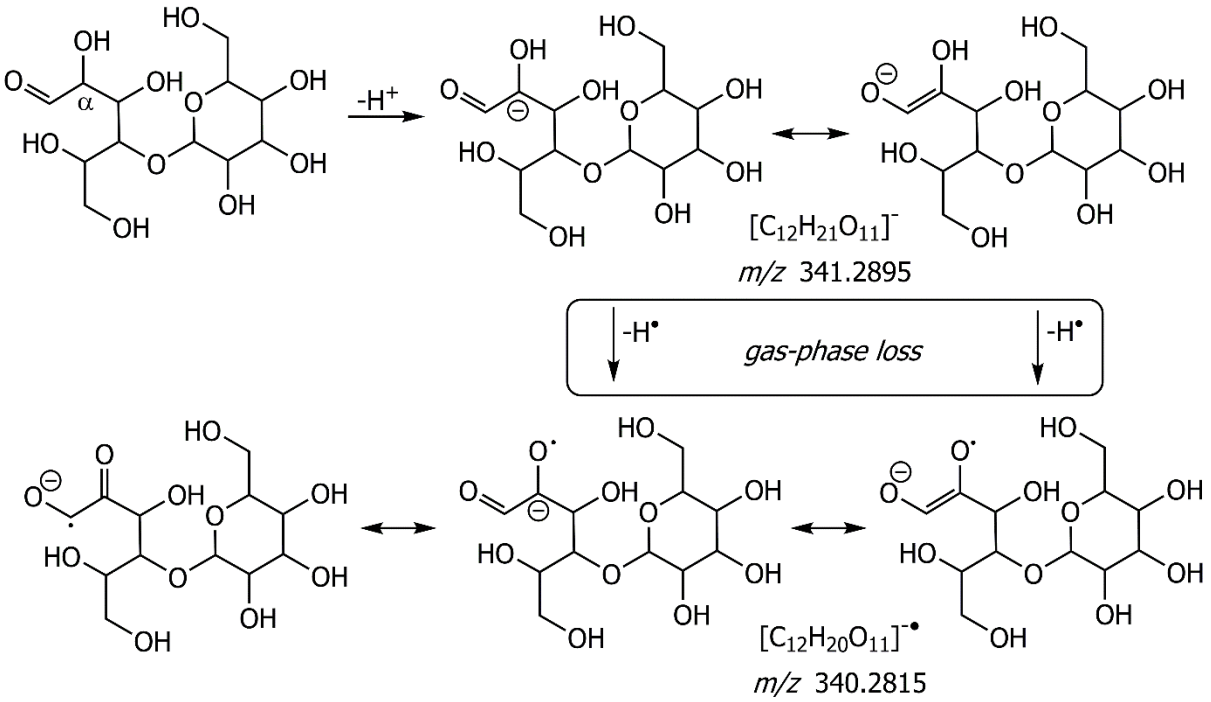

Scheme 3. Suggested formation of radical anions $[M–H^{\bullet}–H]^{-\bullet}$ from deprotonated reducing disaccharides during the MALDI process investigated in this study. In the gas-phase, the hydrogen atom ($H^{\bullet}$) is presumably lost from the hydroxyl group in the α carbon.

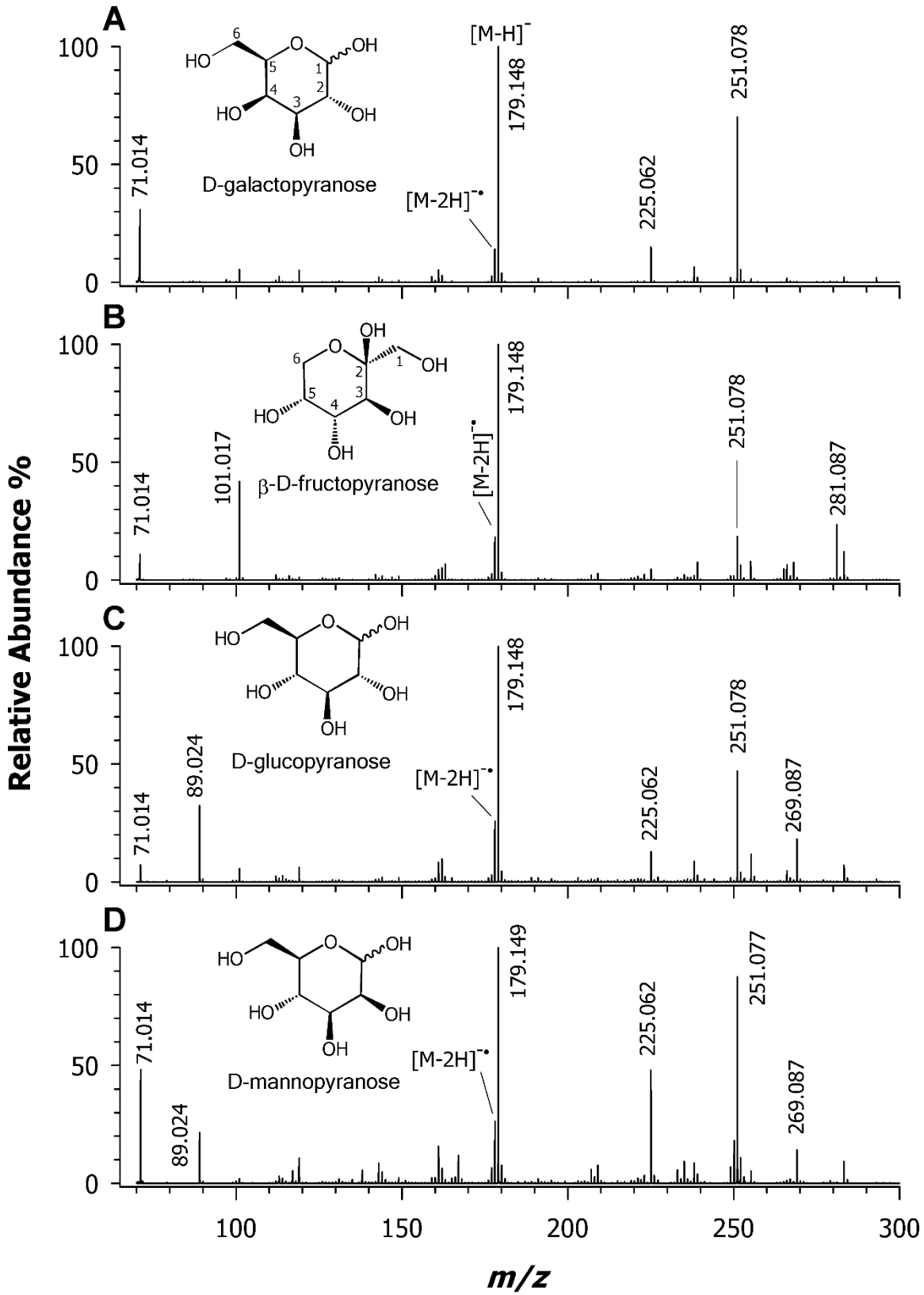
A
B
C
D
Relative Abundance %
m/z
D-galactopyranose
β-D-fructopyranose
D-glucopyranose
D-mannopyranose
[M-H]⁻
[M-2H]⁻•
71.014
89.024
101.017
179.148
179.149
225.062
251.078
251.077
269.087
281.087

Figure 1

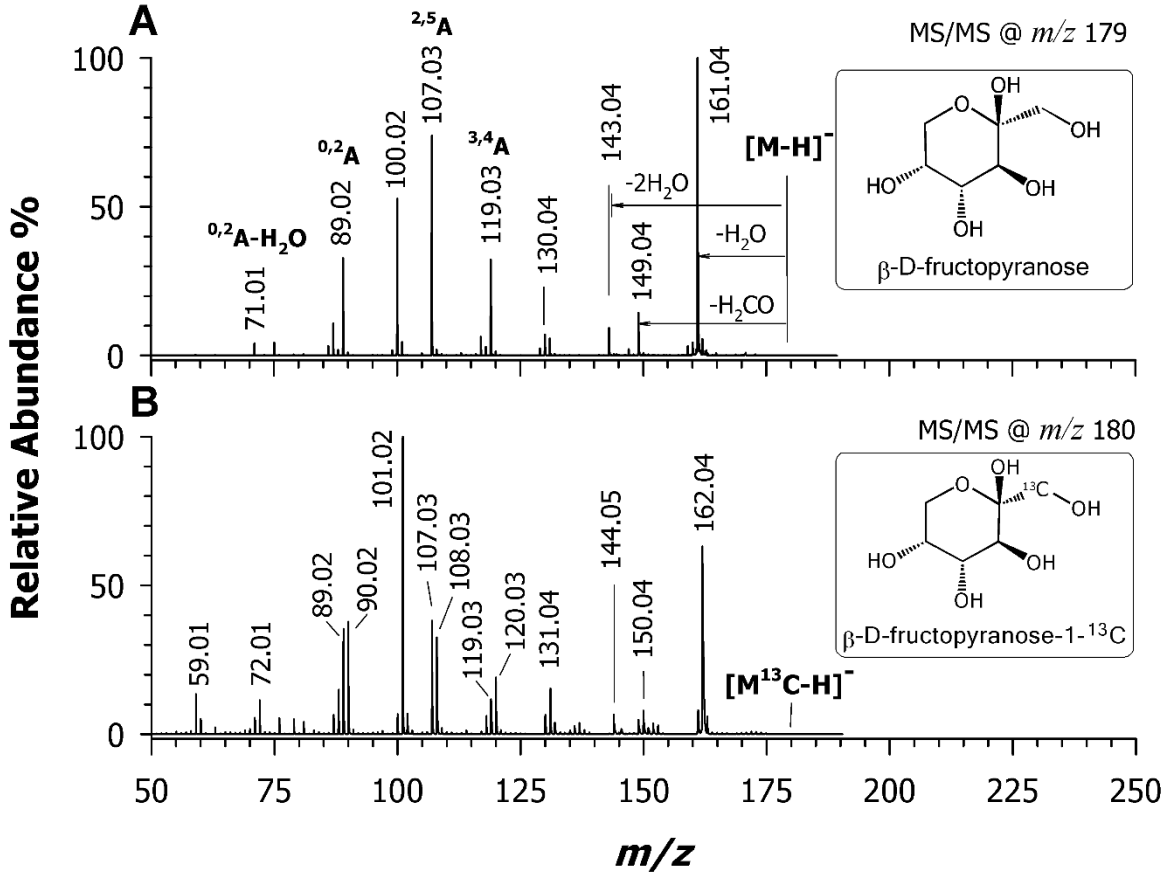
A
MS/MS @ m/z 179
β-D-fructopyranose
B
MS/MS @ m/z 180
β-D-fructopyranose-1-13C
Relative Abundance %
m/z
[M-H]-
[M13C-H]-
0,2A-H2O
0,2A
2,5A
3,4A
-2H2O
-H2O
-H2CO

Figure 2

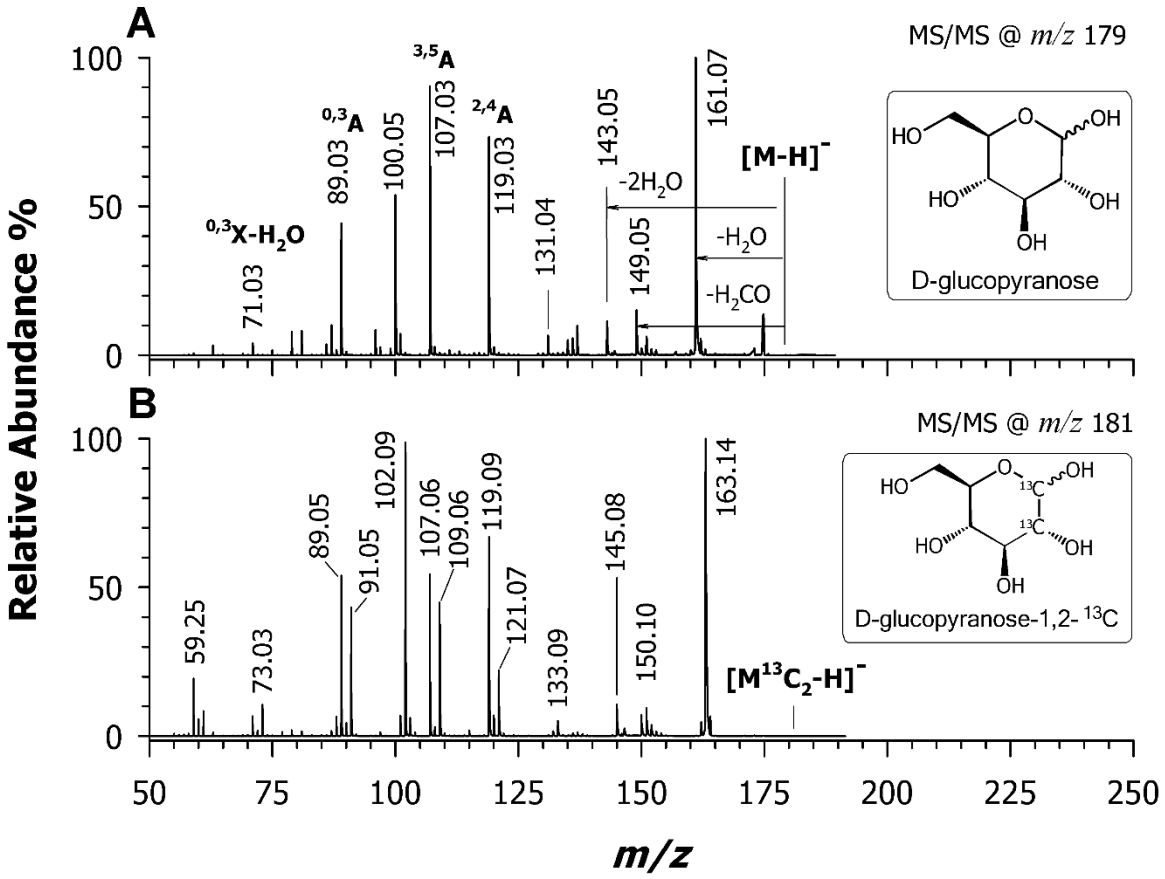
A
MS/MS @ m/z 179
100
50
0
Relative Abundance %
0,3X-H2O
71.03
0,3A
89.03
100.05
3,5A
107.03
2,4A
119.03
131.04
143.05
149.05
161.07
-2H2O
-H2O
-H2CO
[M-H]-
HO
O
OH
HO
OH
OH
D-glucopyranose
B
MS/MS @ m/z 181
59.25
73.03
89.05
91.05
102.09
107.06
109.06
119.09
121.07
133.09
145.08
150.10
163.14
[M13C2-H]-
13C
D-glucopyranose-1,2- 13C
50
75
100
125
150
175
200
225
250
m/z

Figure 3

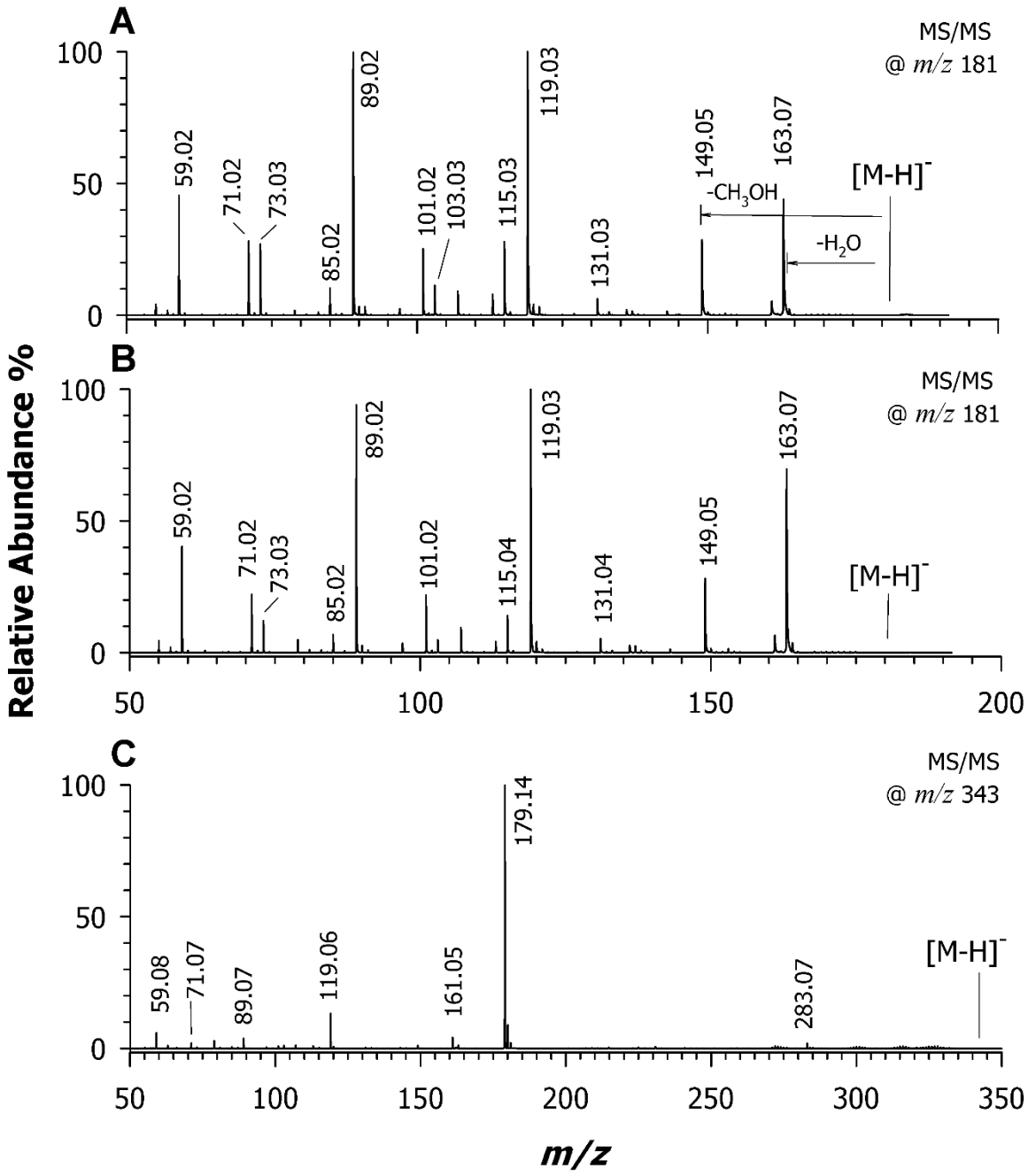
A
MS/MS
@ m/z 181
100
50
0
59.02
71.02
73.03
85.02
89.02
101.02
103.03
115.03
119.03
131.03
149.05
163.07
-CH3OH
-H2O
[M-H]-
B
MS/MS
@ m/z 181
59.02
71.02
73.03
85.02
89.02
101.02
115.04
119.03
131.04
149.05
163.07
[M-H]-
Relative Abundance %
C
MS/MS
@ m/z 343
59.08
71.07
89.07
119.06
161.05
179.14
283.07
[M-H]-
50
100
150
200
250
300
350
m/z

Figure 4

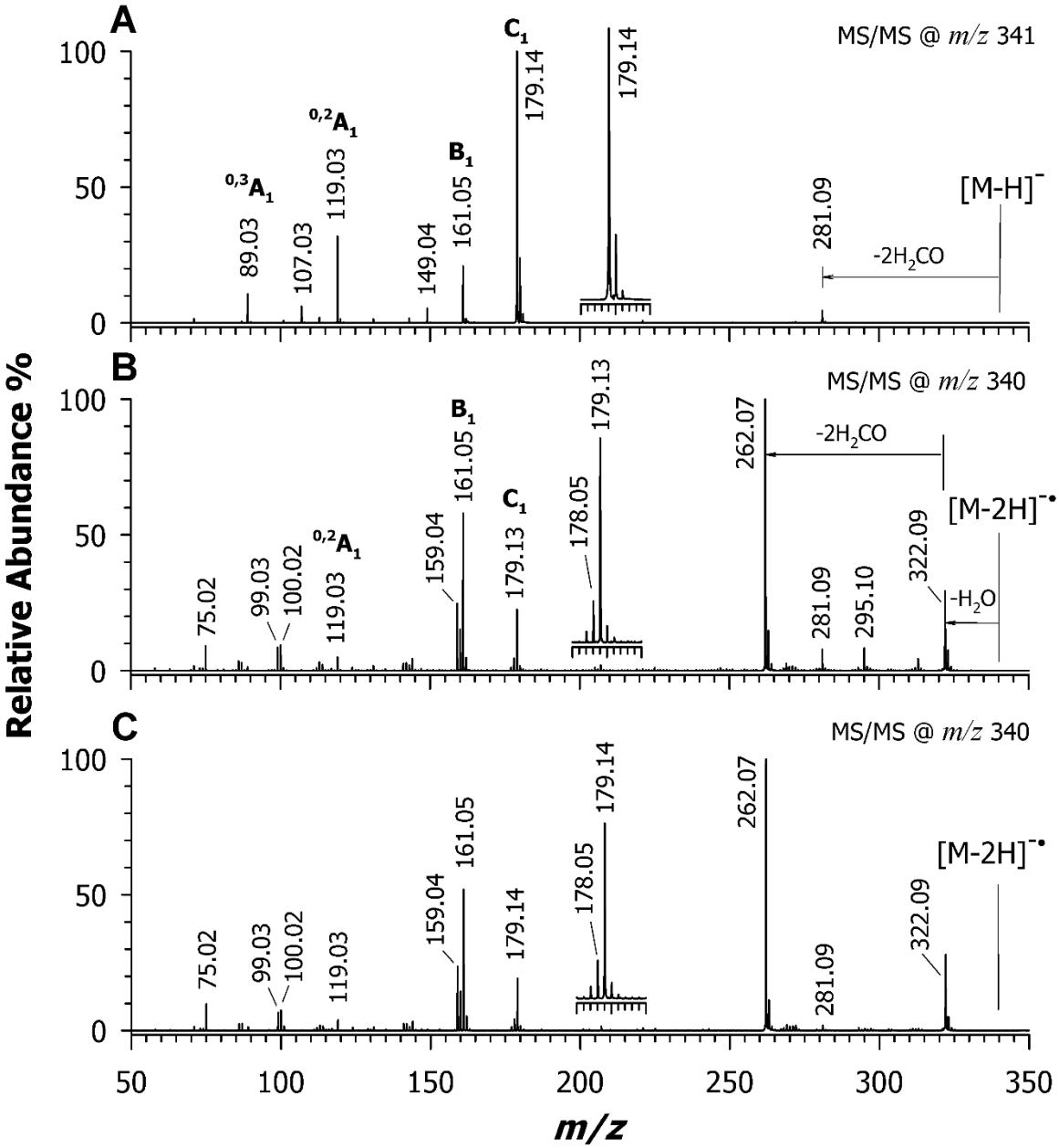
A
MS/MS @ m/z 341
B
MS/MS @ m/z 340
C
MS/MS @ m/z 340
Relative Abundance %
m/z
[M-H]⁻
[M-2H]⁻•
-2H2CO
-H2O

Figure 5

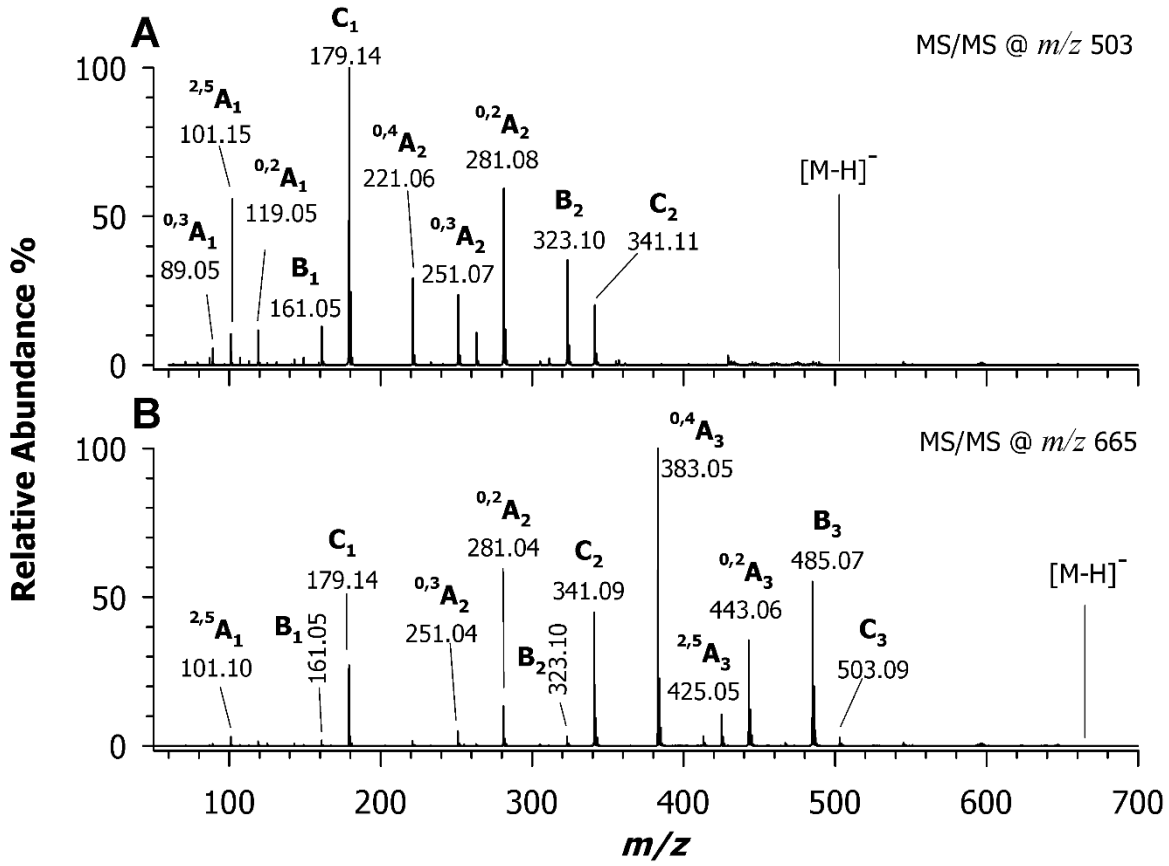
A
MS/MS @ m/z 503
C1
179.14
2,5A1
101.15
0,2A1
119.05
0,4A2
221.06
0,2A2
281.08
0,3A1
89.05
B1
161.05
0,3A2
251.07
B2
323.10
C2
341.11
[M-H]-
B
MS/MS @ m/z 665
0,4A3
383.05
0,2A2
281.04
C1
179.14
C2
341.09
B3
485.07
0,2A3
443.06
[M-H]-
0,3A2
251.04
2,5A1
101.10
B1
161.05
B2
323.10
2,5A3
425.05
C3
503.09
Relative Abundance %
100
50
0
100
200
300
400
500
600
700
m/z

Figure 6

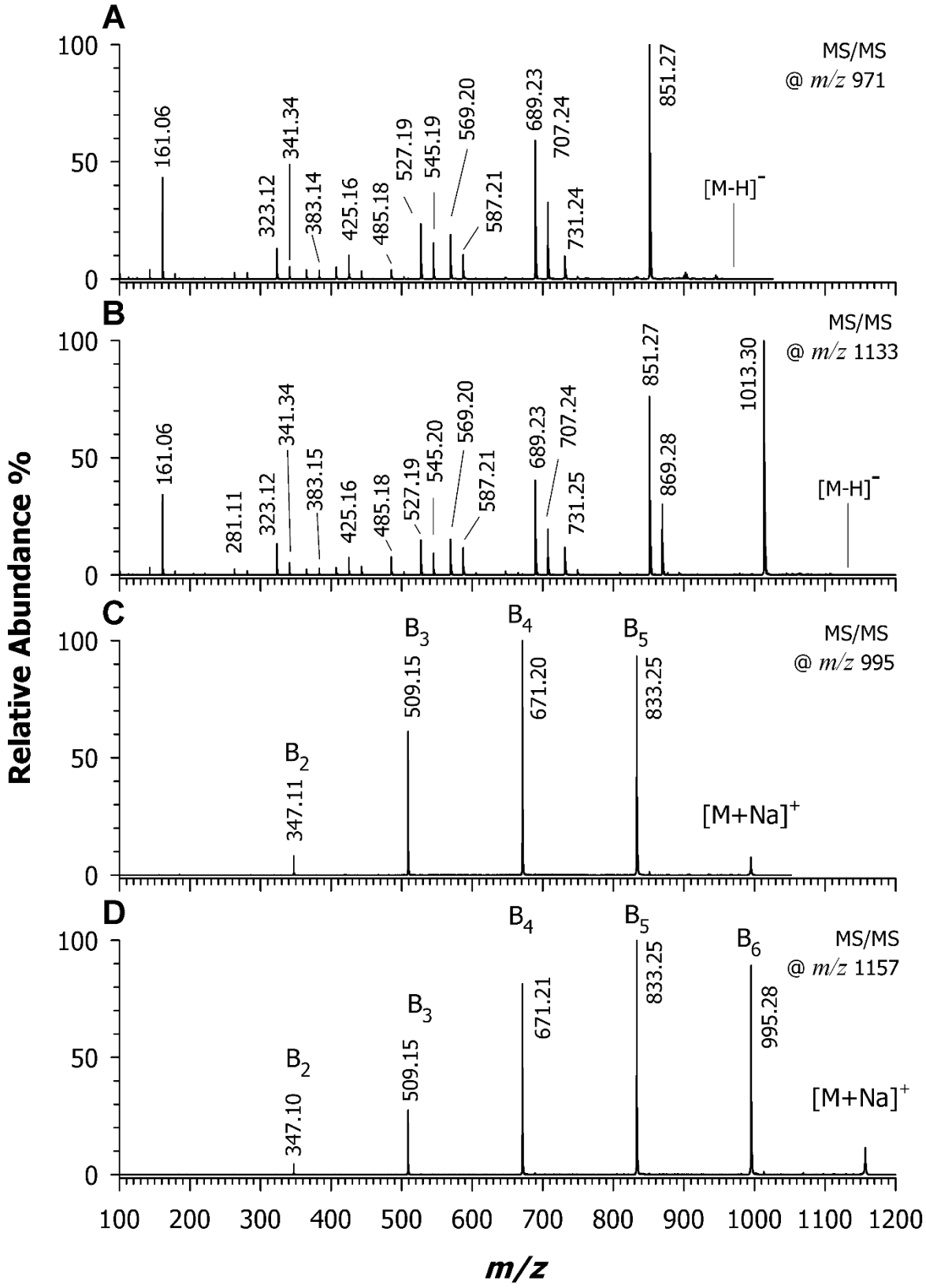
A
MS/MS
@ m/z 971
161.06
323.12
341.34
383.14
425.16
485.18
527.19
545.19
569.20
587.21
689.23
707.24
731.24
851.27
[M-H]-
B
MS/MS
@ m/z 1133
161.06
281.11
323.12
341.34
383.15
425.16
485.18
527.19
545.20
569.20
587.21
689.23
707.24
731.25
851.27
869.28
1013.30
[M-H]-
C
MS/MS
@ m/z 995
B2
347.11
B3
509.15
B4
671.20
B5
833.25
[M+Na]+
D
MS/MS
@ m/z 1157
B2
347.10
B3
509.15
B4
671.21
B5
833.25
B6
995.28
[M+Na]+
Relative Abundance %
m/z
100
200
300
400
500
600
700
800
900
1000
1100
1200
0
50
100

Figure 7